JMEPEG (2011) 20:1423–1437
DOI: 10.1007/s11665-010-9704-3

1059-9495/$19.00

Design of Experiments Study of Hydroxyapatite Synthesis for Orthopaedic Application Using Fractional Factorial Design

S. Kehoe, M. Ardhaoui, and J. Stokes

(Submitted February 6, 2009; in revised form April 8, 2010)

Hydroxyapatite, (HAp), $Ca_{10}(PO_4)_6(OH)_2$, is a naturally occurring mineral found in the inorganic component of enamel and human bone, consequently the present research focus is its ability to promote bone growth onto femoral implants when the HAp powder is sprayed using plasma thermal spraying. As the sprayed deposit requires certain mechanical and biological performances, the characteristics of the starting HAp powder will provide these properties. Hap powders were synthesized via a wet chemical precipitation technique using a Fractional Factorial, Resolution IV, two-level experimental design to evaluate the critical process parameters (reagent addition rate, reaction temperature, stirring speed, ripening time, initial calcium concentration, and the presence of an inert atmosphere) and their effect (main and interaction) on the final HAp powder characteristics, such as, phase composition, purity, crystallinity, crystallite size, lattice parameters, particle size, and particle size distribution. All six selected variables investigated, showed an influence (either as a minor or major significance) on one or more of the responses investigated, either as a main or interaction effect. However, both the ripening time and the stirring speed were found to significantly affect the majority of the five responses, with the reaction temperature also having a significant effect on the final phase composition, lattice parameters, and particle size.

Keywords chemical precipitation, design of experiments, fractional factorial, hydroxyapatite, screening

1. Introduction

Hydroxylapatite (HA) has the chemical formula of $Ca_5(OH)(PO_4)_3$ (Ref 1); but is more commonly written as the chemical formula $Ca_{10}(PO_4)_6(OH)_2$, Hydroxyapatite (HAp), to denote that the crystal unit cell comprises of two molecules at pH > 4.2 (Ref 2). HAp and other related calcium phosphate minerals have been utilized extensively as implant materials for many years due to their identical chemical composition and high biocompatibility with natural bone. HAp does not exhibit any cytotoxic effects. Moreover, it can promote new bone growth, in what is more commonly termed an osteoconductive process. The performance, lifespan, and quality of the biological coating in vivo are largely dependent on powder morphology, phase composition, particle size, and crystallinity (Ref 3). In literature, several methods to prepare HAp crystals have been reported, including solid state reactions, crystal growth under hydrothermal conditions, layer hydrolysis of other calcium phosphate salts, sol-gel crystallization and precipitation methods (Ref 3, 4). Variations in parameters that affect the synthesis are necessary to produce HAp of desired powder characteristics, such as crystallinity, phase composition, particle size, and specific surface area (Ref 5, 6). Essentially, the synthesis of HAp crystals from supersaturated aqueous solutions is advantageous due to its low cost and simplicity (Ref 3), but most of the synthetic routes for preparing HAp result in the formation of non-stoichiometric products (Ref 7). Deviation from stoichiometric HAp is due to the presence in the crystal lattice of vacancies and ion substitutes such as carbonates, hydrogen phosphates, potassium, sodium, nitrates, and chloride, which are usually introduced into the precipitating system with the reactants. Contamination of HAp with these ions or formation of deficient hydroxyapatites suffers from significant changes in their crystallographic characteristics and have different crystal morphology as compared to stoichiometric HAp (Ref 7). Difficulties encountered in preparing synthetic HAp crystals from aqueous solutions are attributed to the high chemical affinity of the material to some ions, the complex nature of the calcium phosphates system, and the role of kinetic parameters. The formation of synthetic HAp crystals from highly supersaturated solutions proceeds via intermediate precursor phases, which have a transitory existence, such as tricalcium phosphate (TCP) and octacalcium phosphate (OCP) (Ref 7).

Implementing the precipitation route involves the reaction of either: (i) diammonium hydrogen phosphate with calcium nitrate or (ii) orthophosphoric acid with calcium hydroxide (Ref 3). The reaction for the method (i) reaction is as follows:

$$10Ca(NO_3)_2 + 6(NH_4)_2HPO_4 + 8NH_4OH \rightarrow Ca_{10}(PO_4)_6(OH)_2 + 20NH_4NO_3 + 6H_2O \quad \text{(Eq 1)}$$

The major disadvantage of this method is that the purity of the precipitated HAp powders is affected by the purity of the

S. Kehoe, M. Ardhaoui, and **J. Stokes**, MPRC, Materials Processing Research Centre, Dublin City University, Dublin 9, Ireland and NCPST, National Centre for Plasma Science and Technology, Dublin City University, Dublin 9, Ireland. Contact e-mail: joseph.t.stokes@dcu.ie.

calcium nitrate. Furthermore, the excess ammonia and ammonium by-products must be removed by extensive washing. In comparison to method (i), method (ii) is a simpler more cost-effective process, suitable for the production of HAp on an industrial scale since its only by-product is water:

$$10Ca(OH)_2+6H_3PO_4 \rightarrow Ca(PO_4)_6(OH)_2+18H_2O \quad \text{(Eq 2)}$$

The major crystalline phases usually present in calcium-phosphate-based powders are HAp, β-tricalcium phosphate (β-TCP), and α-tricalcium phosphate (α-TCP). The most stable phase is HAp, while α-TCP and β-TCP are biodegradable (Ref 8).

Xu et al. (Ref 5) synthesised HAp powder particles using the precipitation approach of method (ii). This was achieved by reacting 0.6 mol of orthophosphoric acid (H_3PO_4) with 1 mol of calcium hydroxide ($Ca(OH)_2$). The precipitation reactants were carried out at 40 ± 5 °C in house and terminated when the pH reached 9 through the addition of H_3PO_4. After the complete mixing of the reactants, the precipitate was stirred for two more hours and left overnight to settle. The so-formed HAp suspension was then transported into a spray dryer, where the atomization and drying processes took place. The spray-dried HAp powders were collected and kept in an oven at 60 °C for 12 h to remove any absorbed moisture. The spray-dried HAp powders were then sieved and particles with a size less than 20 μm were heat-treated at 1000 °C for 5 h to increase the thermal stability of the HAp feedstock. A similar approach was taken by Kumar et al. (Ref 6), who also produced HAp powders using the precipitation reaction of method (ii) by reacting orthophosphoric acid (H_3PO_4) with calcium hydroxide. H_3PO_4 was added drop-wise at a rate of 1.5 L/h into a bath of calcium hydroxide maintained at 40 °C until reaching a pH of about 8. The suspension was stirred for 2 h and left to settle overnight. Centrifugation was used, as opposed to the spray-drying method employed by Xu et al. (Ref 5). Polymethyl methacrylate (PMMA) was added as a deflocculant to reduce the HAp slurry viscosity.

In this research, the chemical precipitation method was used to obtain pure, stoichiometric, and crystalline HAp is based on the reaction of orthophosphoric acid with calcium hydroxide (Eq 2). Since calcium-deficient HAp powder is a serious disadvantage, as non-stoichiometric HAp decomposes, during heat treatments, to more soluble solid phases. The aim of this research is to examine the influence of influential process variables on HAp physicochemical properties and determine an optimum set of process variables to produce HAp powder of desired characteristics for optimum coating application using thermal spray application onto femoral implants, to satisfying regulatory requirements (Ref 9-12). Initially, a screening design of experiments was conducted to identify the most influential critical process parameters and their effect (main and interaction) as found from literature (Ref 3, 6, 13-18) on controlling the final HAp powder characteristics, such as phase composition, purity, crystallinity, crystallite size, lattice parameters, particle size, and particle size distribution. Another goal of this research is to apply Design of Experiments (DoE) to develop mathematical models, in terms of the chemical precipitation process parameters.

2. Materials and Methods

The screening DoE experimental plan was based on the Fractional Factorial (Res_{IV}^{4-1}) design (2^{k-n}, $k = 6$ and $n = 2$; size of the fraction used; that is a quarter of a full factorial design of 64 experimental runs) using 16 experimental runs, with main and interaction effects evaluated, using Design Expert 7.1. software (Stat-Ease) to investigate the optimum HAp synthesis process parameters using the chemical precipitation route. The factors were investigated at two levels (+1(high) and −1(low)) and included, reaction synthesis temperature during precipitation, stirring speed, ripening time, acid addition rate, initial calcium concentration, and atmospheric environment (synthesis with and without a controlled atmospheric environment), and were based on a critical review of previous research summarized by the findings shown in Table 1. This experimental design was used to identify the factors which have the most significant effect on the resulting HAp powder properties, such as phase purity, crystallinity, crystallite size (L_{002} and L_{300}), lattice parameters, and particle size. This enabled a quantitative understanding of the relationship and interactions between the process parameters and their final HAp powder properties obtained. The six experimental precipitation process parameters (factors, as found from literature), discussed above, were selected, each one at two levels, and these are indicated in Table 2.

Since the chemical precipitation route for the synthesis or phase evolution of HAp occurs in an aqueous suspension (analogous to that of room temperature (~25 °C), a lower synthesis temperature of 20 °C was chosen as the minimum temperature of synthesis and 60 °C as the maximum, to investigate a broad region outside of the optimum synthesis temperature, as highlighted in existing literature (40 °C)

Table 1 Comparative analysis of previous investigated chemical precipitation process parameters

	Process variables				
Literature source	**Ca/P molar ratio**	**Acid addition rate**	**Stirring speed, rpm**	**Temperature, °C**	**pH**
Kweh et al. (Ref 3)	1.67	-	-	-	9
Kumar et al. (Ref 13)	-	1.5 L/h	-	40	8
Afshar et al. (Ref 14)	1.667	1-2 drops/s	500-2400	40 ± 2	7.5-9
Saeri et al. (Ref 15)	1.667	1-2 drops/s	2400	40 ± 2	7.5
Conn et al. (Ref 16)	1.667	70.8 kg/h	High	20-50	9.5-11; 7.0-7.4
Smiciklas et al. (Ref 17)	1.55-1.71	1-10 mL/min	100-300	25-95	7.0
Lazic et al. (Ref 18)	1.667	-	-	22-95	9.5-12

- Denotes data unpublished

(Ref 5, 14, 15, 19). The stirring speed was set according to limits previously published (Ref 20). During precipitation, absorption of atmospheric CO_2 may occur, which in the form of CO_3^{2-} anion can be incorporated into the apatite crystal lattice. Experiments were performed with or without inert atmosphere to examine the significance of this parameter. Aging time plays an important role in the formation of highly crystallized products through phase evolution. During maturation, aggregation and crystal growth take place in the first 20 h, after precipitation. After 20 h, the crystal length and width are not significantly changed, and due to negative HAp solubility coefficient, this effect is more pronounced at room temperature (Ref 20). Hence, an aging time of 48 h was investigated to examine whether any significant changes occur after this stage. The reaction yield and the reaction vessel capacity were taken into account in setting the minimum and the maximum molar concentrations of reagents: $Ca(OH)_2$ and H_3PO_4. The raw materials $Ca(OH)_2$ and H_3PO_4 react at a molar ratio of 5:3, according to Eq 2.

A second-order linear polynomial (regression) model for the six factors investigated was used to describe the relationship for each of the several responses and tested factors, as follows:

$$Y = b_0 + \sum b_j X_j + \sum b_{ij} X_i X_j + \varepsilon \quad \text{(Eq 3)}$$

where i, j vary from 1 to the number of process variables; coefficient b_0 is the mean of responses of all the experiment; b_i coefficient represents the effect of the variable X_i, and b_{ij} is the coefficient of regression which represents the effects of interactions of variables X_iX_j and ε is the experimental error, such that:

$$\begin{aligned} Y_1 = {} & C_{st} + \beta_1 T_0 + \beta_2 V_{ac} + \beta_3 V_{st} + \beta_4 t_r + \beta_5 Ca^{2+} \\ & + \beta_6 atm. + \beta_7 T_0 * V_{ac} + \beta_8 T_0 * V_{st} + \beta_9 T_0 * t_r \\ & + \beta_{10} T_0 * Ca^{2+} + \beta_{11} T_0 * atm. + \beta_{12} V_{ac} * V_{st} \\ & + \beta_{13} V_{ac} * t_r + \beta_{14} V_{ac} * Ca^{2+} + \beta_{15} V_{ac} * atm. \\ & + \beta_{16} V_{st} * t_r + \beta_{17} V_{st} * Ca^{2+} + \beta_{18} V_{st} * atm. \\ & + \beta_{19} t_r * Ca^{2+} + \beta_{20} t_r * atm. + \beta_{21} Ca^{2+} * atm. \\ & + \text{experimental error} \end{aligned} \quad \text{(Eq 4)}$$

where Y_1 is response 1, β_1-β_{21} is the regression co-efficient, T_0 is the reaction synthesis temperature, V_{ac} is the acid addition rate, V_{st} is the stirring speed, t_r is the ripening time, Ca^{2+} is the initial calcium concentration and atm. is the atmospheric control. This model was used to evaluate all the responses (Y_1-Y_6) such as Y_1 the phase purity, X_p (%), Y_2 the crystallinity, X_c (%), Y_3 the crystallite size in the 002 plane, X_s, L_{002} (nm), Y_4 the crystallite size in the 300 plane, X_s, L_{300} (nm), Y_5 the a/c ratio, and Y_6 the particle size, P_s, (μm). The responses were measured in sequential order for each experiment and performed in triplicate.

The matrix of experiments obtained according to the Fractional-Factorial design is shown in Table 3. The experiments were performed in random order to ensure that uncontrolled factors did not influence the results. Figure 1 illustrates an overview of the complete production process to prepare HAp powder from aqueous suspension via chemical precipitation. The factors and responses are presented for the stages of the process, in which they are controlled and evaluated, respectively, according to Table 3.

0.1-2 M $Ca(OH)_2$ solutions were prepared by adding CaO powders to 500 mL of distilled water in a 1000 mL enclosed reactor and vigorously stirred with a vertical mechanical overhead stirrer between 600 and 1500 rpm at the reaction temperature (20-100 °C) maintained by a thermostat-controlled water-bath. The H_3PO_4 acid was added to the $Ca(OH)_2$ solution at an addition rate of 0.005-0.01 mol/min using a peristaltic pump. Ripening periods of between 0.5 and 48 h were investigated to

Table 2 Experimental factors and level of factors

No	Variable	Symbol	Level −1	Level +1
A	Reagent addition rate, mol/min	V_{ac}	0.005	0.01
B	Temperature, °C	T_0	20	60
C	Stirring speed, rpm	V_{st}	600	1500
D	Ripening time, h	t_r	0.5	48
E	Initial Ca^{2+} concentration, mol/L	Ca^{2+}	0.1	2
F	Inert atmosphere	atm.	Without N_2	With N_2

Table 3 Design matrix for screening fractional factorial design, expressed as real values

Exp no.	Run order	H_3PO_4 addition rate, mol/min	Temperature, °C	Stirring speed, rpm	Ripening time, h	Calcium concentration, mol/L	Inert atmosphere
N1	15	0.005	20	600	0.5	0.1	Yes
N2	4	0.01	20	600	0.5	2	Yes
N3	10	0.005	60	600	0.5	2	No
N4	8	0.01	60	600	0.5	0.1	No
N5	5	0.005	20	1500	0.5	2	No
N6	3	0.01	20	1500	0.5	0.1	No
N7	16	0.005	60	1500	0.5	0.1	Yes
N8	1	0.01	60	1500	0.5	2	Yes
N9	6	0.005	20	600	48	0.1	No
N10	2	0.01	20	600	48	2	No
N11	12	0.005	60	600	48	2	Yes
N12	14	0.01	60	600	48	0.1	Yes
N13	11	0.005	20	1500	48	2	Yes
N14	13	0.01	20	1500	48	0.1	Yes
N15	7	0.005	60	1500	48	0.1	No
N16	9	0.01	60	1500	48	2	No

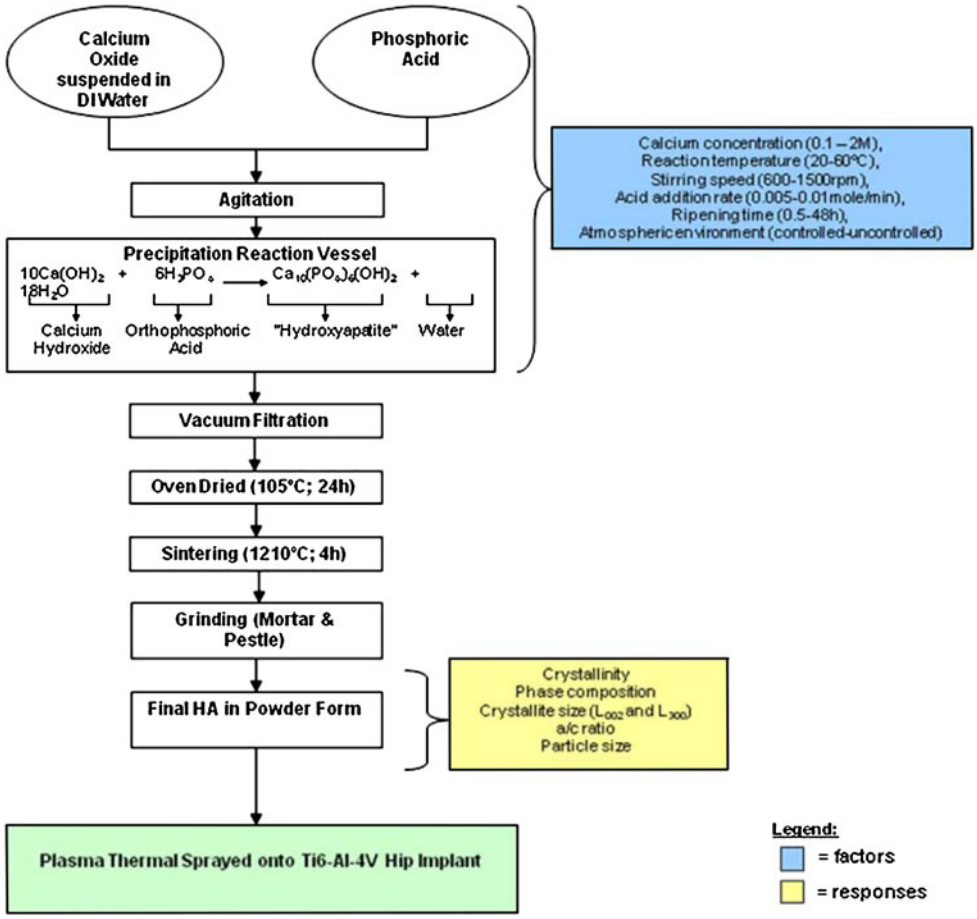

Fig. 1 Overview of the production process in obtaining HAp in powder form and the process variables and responses evaluated at the screening fractional factorial design stage

monitor the maturation of HAp in the reaction vessel, while kept under continuous stirring conditions and reaction temperature (as dictated by the experimental design). At the end of this ripening period, the aqueous suspension of HAp was filtered from suction via vacuum filtration and oven-dried at 105 °C for 24 h. Finally, all the samples were sintered at 1210 °C for 4 h to increase the final crystallinity obtained (ideally, >95%), ground using a mortar and pestle and sieved for particle size not exceeding 100 μm (to suit plasma thermal spraying application).

Phase analysis of the HAp powder particles was performed on a Bruker Advance D8 XRD using monochromated CuKα radiation at 40 kV and 40 mA. The scanning range (2θ) was performed from 20° to 60° with a step size of 0.02° 2θ/s. XRD was used to evaluate the phases present (X_p) and determine crystallographic properties of the HAp powders to ensure compliance to regulatory requirements. Phase identification was performed with reference to the library database supplied by the International Centre for Diffraction Data (ICDD) by directly comparing the X-ray diffraction patterns to the Joint Committee for Powder Diffraction Standards (JCPDS) files for HAp (JCPDS, Card No. 9-432) and also the common phases present within calcium-phosphate-based powders, such as α-TCP (9-348), β-TCP (9-169), DCPA (9-80), DCPD (9-77), OCP (26-1056), TTCP (25-1137), and CHAp (19-272), to obtain an indication of the relative proportions of phases present in the powders analyzed. The percentage crystallinity (X_c) was determined using the following equation (Ref 7, 21):

$$X_c\ (\%) = \frac{\sum A_C}{\sum A_C + \sum A_A} \times 100 \qquad \text{(Eq 5)}$$

where $\Sigma A_C + \Sigma A_A$ give the sum of the area under all the HAp crystalline and amorphous peaks and ΣA_C yields the sum of the areas under the crystalline peaks present in the scan range between 20° and 60°. The X-ray diffraction data was used to assess crystallite size (L_{002} and L_{300}) based on Scherrer's formula (see Eq 6) from XRD peak broadening as follows (Ref 7, 17):

$$D = 0.9\alpha\ \mathrm{FWHM}\cos\theta \qquad \text{(Eq 6)}$$

where D is the crystallite size (nm), α the wavelength of monochromatic X-ray beam (0.15406 nm for Cu Kα radiation), FWHM is the full width at the half maximum of the diffraction peak under consideration (rad), and θ the diffraction angle (°). Lattice parameters, along the a and c axes were determined using unit cell refinement software package CelRef 3.0. Particle size (P_s) analysis was carried out with a Malvern Mastersizer to study the HAp powder particle sizes.

3. Experimental Results and Discussion

The results of the screening stage of the two-level fractional-factorial experimental design are presented in Table 4. Analysis

Table 4 Phase purity (X_p), crystallinity (X_c), crystallite size (X_s, L_{002}, and L_{300}), lattice parameter ratio (a/c), and mean particle size (P_s) of the different HAp samples for various conditions of acid addition (V_{ac}), temperature (T_0), stirring speed (V_{st}), ripening time (t_r), calcium concentration (Ca^{2+}) and atmospheric control (atm.)

Sample	Purity, X_p, %	Crystallinity, X_c, %	Crystallite size, X_s		Lattice parameter, a	Lattice parameter, c	Mean particle size, P_s, μm
			L_{002}, nm	L_{300}, nm			
N1	44.25	72.23	61.47	56.09	9.4243	6.8953	58.60
N2	21.15	80.62	59.44	66.91	9.4625	6.8965	38.03
N3	83.19	45.69	90.48	126.35	9.4805	6.9049	23.28
N4	65.02	67.38	54.50	86.23	9.4828	6.8814	48.82
N5	44.01	54.85	98.79	139.70	9.4072	6.8817	54.94
N6	42.29	57.68	76.03	82.49	9.4168	6.8570	57.77
N7	63.59	76.49	59.04	87.96	9.4312	6.8890	19.96
N8	50.21	61.29	51.44	64.35	9.4462	6.8961	22.65
N9	86.37	58.50	41.60	58.84	9.4264	6.8749	63.83
N10	44.88	73.21	54.77	10.73	9.4871	6.8882	30.81
N11	74.85	71.74	60.82	73.91	9.4255	6.8820	20.74
N12	53.77	79.65	44.28	75.14	9.4300	6.8819	50.69
N13	38.14	80.58	52.20	70.61	9.4150	6.8808	34.38
N14	100.00	86.32	57.11	64.25	9.4145	6.8805	53.48
N15	44.27	90.95	69.45	76.04	9.4173	6.9009	36.15
N16	98.89	95.19	107.92	90.53	9.4296	6.8723	15.38

of the regression coefficients of the linear polynomial models describing the relationship between the responses of phase purity (X_p), crystallinity (X_c), crystallite sizes (X_s, L_{002}, and L_{300}), lattice parameters (a and c), and mean particle size (P_s) against the six factors (V_{ac}, T_0, V_{st}, t_r, Ca^{2+}, and atm.) is presented in the following sections.

3.1 Phase Purity Model Development

By selecting the backward regression method, the insignificant model terms ($P < 0.05$), were automatically eliminated. The ANOVA results for the phase purity showed a significant model, plus accounting for other adequacy measures like R^2 (0.9951), adjusted R^2 (0.9853) and predicted R^2 (0.9498). The adequate precision in this case was 34.562, where an adequate precision ratio of greater than 4 indicated adequate model discrimination (Ref 22), also supported by Fig. 2(a) the relationship between the actual and predicted values of phase purity (since the residuals in the prediction of each response are small, with the residuals tending to be close to the diagonal line). The ANOVA indicates that for the phase purity model, all the chemical precipitation parameters have an effect on the resulting phase purity model, either as a main or an interaction effect with another parameter. The main effects of the reaction synthesis temperature (T_0), ripening time (t_r), calcium concentration (Ca^{2+}), presence of an atmospherically controlled environment (atm.), and the two-way interaction effects of acid addition rate and stirring speed ($V_{ac} * V_{st}$), acid addition rate and ripening time ($V_{ac} * t_r$), acid addition rate and calcium concentration ($V_{ac} * Ca^{2+}$), reaction temperature and ripening time ($T_0 * t_r$), reaction temperature and a controlled environment ($T_0 *$ atm.), and the three-way interaction of acid addition rate, reaction temperature, and controlled environment ($V_{ac} * T_0 *$ atm.) are the most significant model terms associated with phase purity. The final mathematical models in terms of coded and actual factors, for an atm. (with or without), as determined by the design expert software are shown in Eq 7 to 9.

$$\begin{aligned}\text{Phase purity, } X_p\ (\%) &= 59.68 + 7.04(T_0) + 7.97(t_r) - 2.76\left(Ca^{2+}\right) + 3.93(\text{atm.}) \\ &\quad + 12.83(V_{ac} * V_{st}) + 6.89(V_{ac} * t_r) - 2.98\left(V_{ac} * Ca^{2+}\right) \\ &\quad - 6.75(T_0 * t_r) + 2.18(T_0 * \text{atm.}) + 9.56(V_{ac} * T_0 * \text{atm.})\end{aligned} \quad \text{(Eq 7)}$$

For an uncontrolled atmospheric environment:

$$\begin{aligned}\text{Phase purity, } X_p\ (\%) &= +70.50227 + 1.9603(\text{reaction temp}) \\ &\quad + 0.032905(\text{ripening time}) + 6.49911\left(Ca^{2+}\ \text{conc.}\right) \\ &\quad + 11.40128(H_3PO_4\ \text{addition rate} * \text{stirring speed}) \\ &\quad + 116.08032(H_3PO_4\ \text{addition rate} * \text{ripening time}) \\ &\quad - 1254.60263\left(H_3PO_4\ \text{addition rate} * Ca^{2+}\ \text{conc.}\right) \\ &\quad - 0.014202(\text{reaction temp} * \text{ripening time})\end{aligned} \quad \text{(Eq 8)}$$

For a controlled (inert) atmospheric environment:

$$\begin{aligned}\text{Phase purity, } X_p\ (\%) &= +188.45472 - 0.68800(\text{reaction temp}) \\ &\quad + 6.49911\left(Ca^{2+}\ \text{conc.}\right) + 0.032905(\text{ripening time}) \\ &\quad + 11.40128(H_3PO_4\ \text{addition rate} * \text{stirring speed}) \\ &\quad + 116.08032(H_3PO_4\ \text{addition rate} * \text{ripening time}) \\ &\quad - 1254.60263\left(H_3PO_4\ \text{addition rate} * Ca^{2+}\ \text{conc.}\right) \\ &\quad - 0.014202(\text{temp} * \text{ripening time})\end{aligned} \quad \text{(Eq 9)}$$

This figure indicates that the developed model is adequate, The pareto chart for the phase purity model, as illustrated in Fig. 3(a), highlights the order of the significant main and

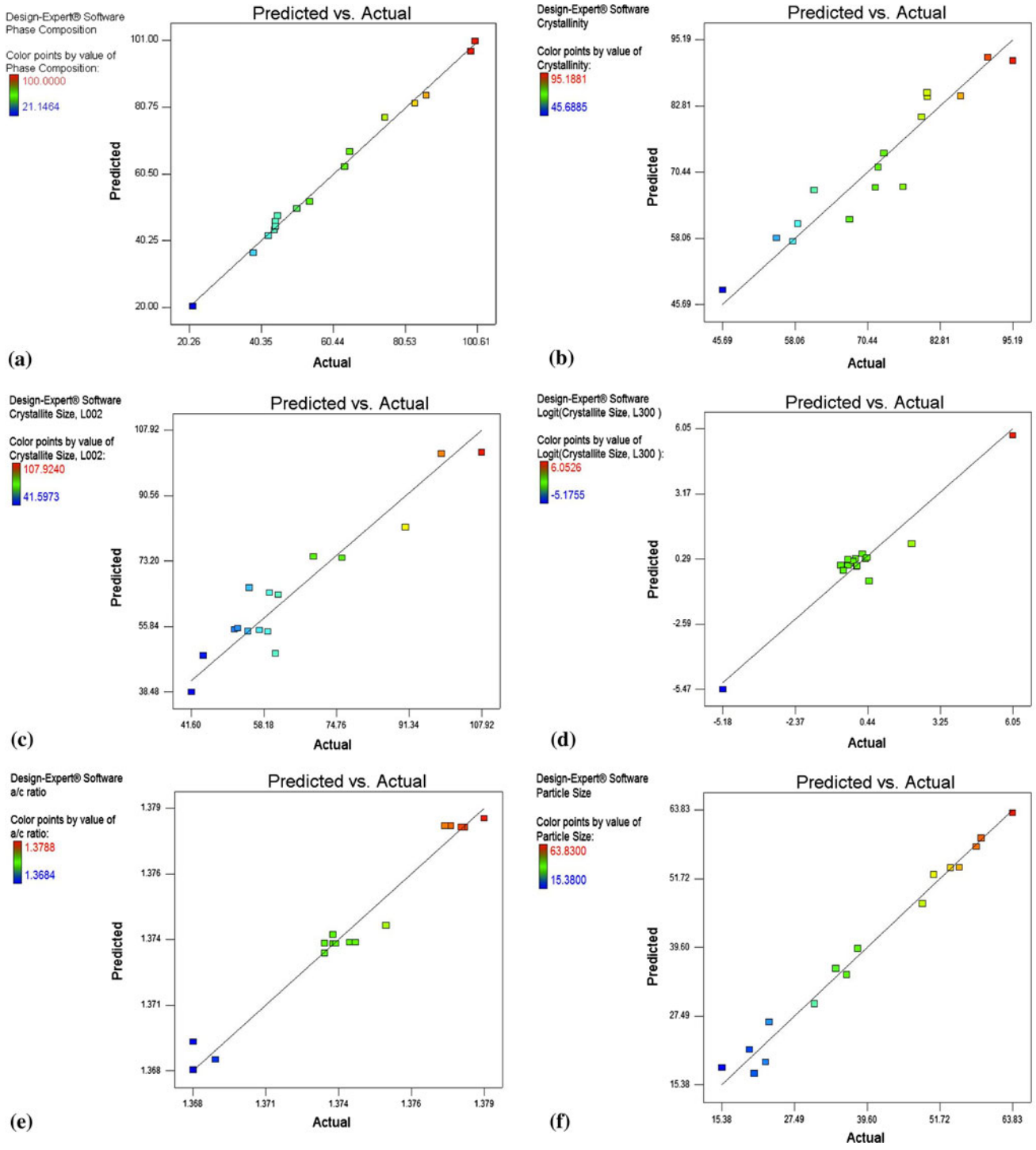

Fig. 2 Scatter diagrams for (a) phase purity, (b) crystallinity, (c) crystallite size, L_{002}, (d) crystallite size, L_{300}, (e) lattice parameter ratio, and (f) particle size

interaction parameter effects, which ultimately affect the phase purity model.

The order of the level of significance of the positive effects of the chemical precipitation process parameters on the phase purity follows the order: $(V_{ac} * V_{st}) > (V_{ac} * T_0 * \text{atm.}) > (t_r) > (T_0) > (V_{ac} * t_r) > (\text{atm.}) > (T_0 * \text{atm.})$, while the order of the level of significance of the negative effects on the phase purity is as follows: $(T_0 * t_r) > (V_{ac} * Ca^{2+}) > (Ca^{2+})$. Hence, if high levels of phase purity are desired, the top four most influencing effects for control are as follows:

1.	Acid addition rate * stirring speed↑	Two-way interaction effect
2.	Acid addition rate * reaction temperature * atmospheric control↑	Three-way interaction effect
3.	Ripening time↑	Main effect
4.	Reaction temperature↑	Main effect

Where ↑ denotes a high level and ↓ denotes a low level is required.

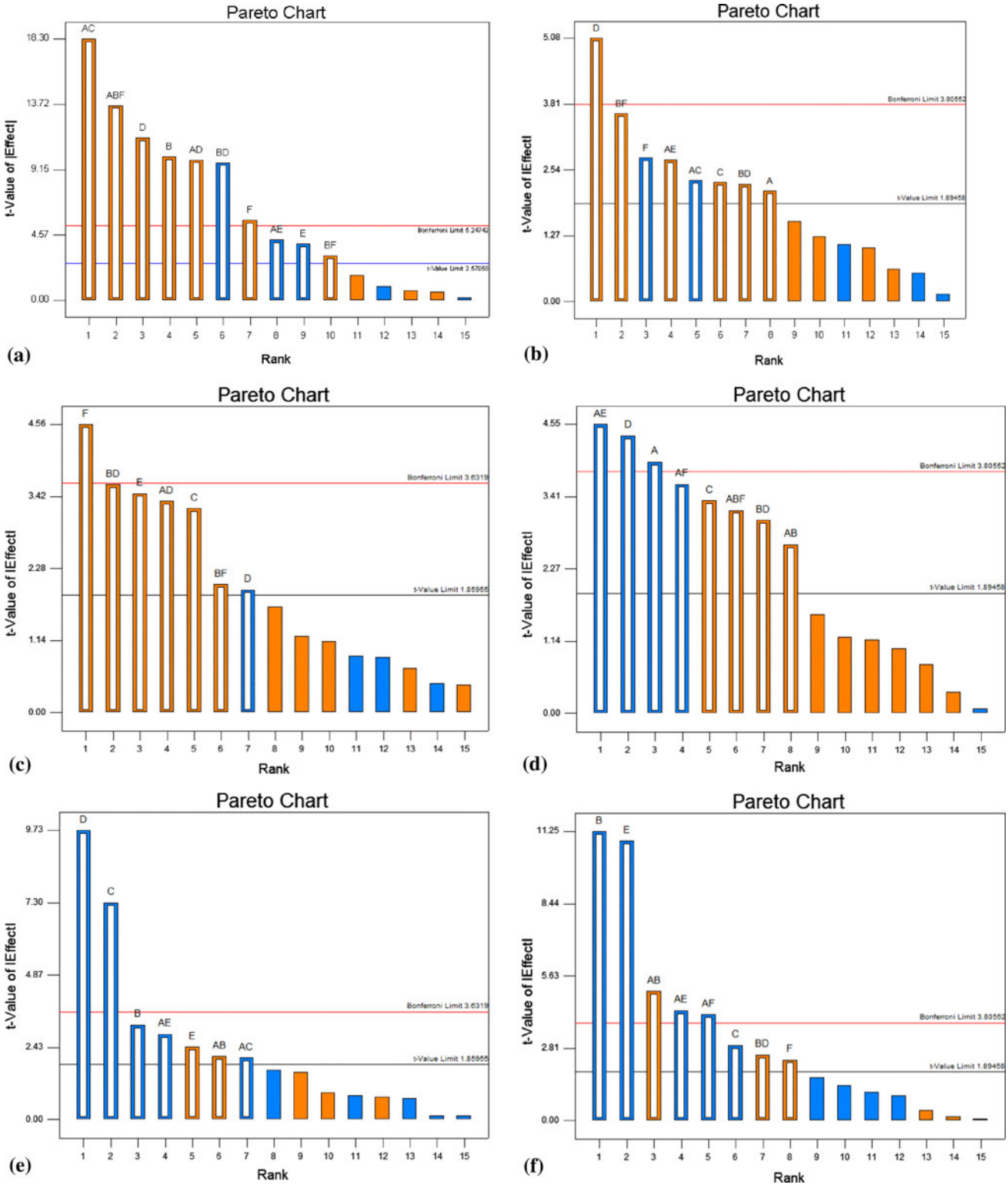

Fig. 3 Pareto charts for (a) phase purity, (b) crystallinity, (c) crystallite size, L_{002}, (d) crystallite size, L_{300}, (e) lattice parameter ratio, and (f) particle size

2-D contour plots are presented in Fig. 4(a) and (b), and highlight the positive influence of increasing both the reaction synthesis temperature and the ripening time. However, a decrease in the calcium concentration is required to ensure high levels of phase purity are attained. A ripening time of at least 24 h proved difficult in attaining a minimum of 95% purity at ambient reaction temperatures. Instead, higher levels of a reaction temperature are necessary to correct this. It is also evident that the presence of a controlled (inert) environment has a positive effect on the final purity obtained. The model also demonstrates that low temperature synthesis at a low stirring speed results in low levels of HAp purity (i.e., a mixture of

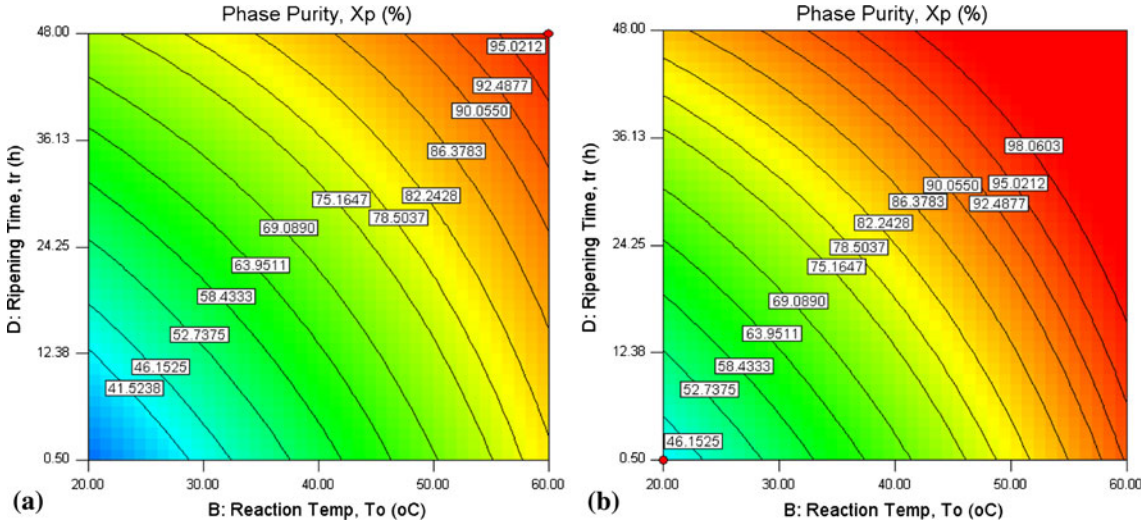

Fig. 4 Contour plots of phase purity at (a) a stirring speed of 600 rpm and (b) a stirring speed of 1500 rpm (under a controlled environment at t_r = 48 h and Ca^{2+} = 2.0 M)

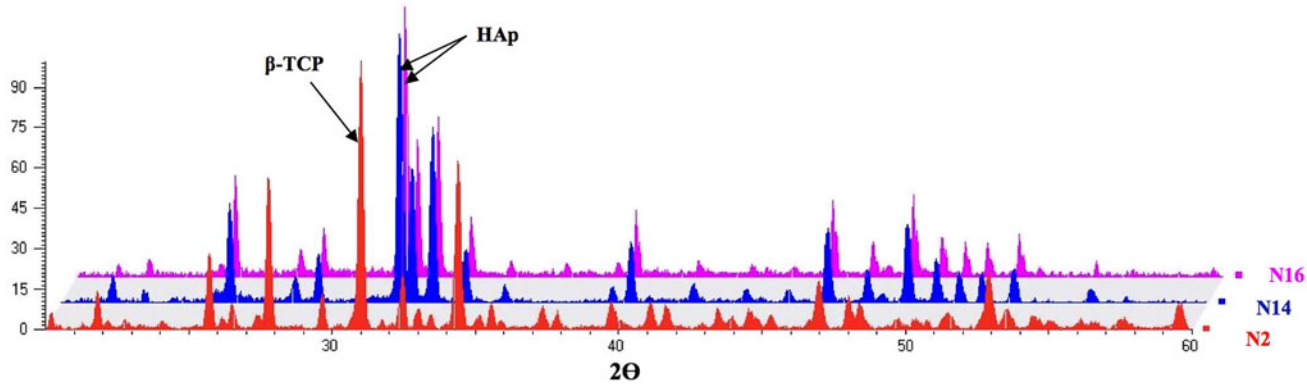

Fig. 5 3-D illustration comparing XRD spectra obtained for N2, N14, and N16

HAp and β-TCP), while using a high synthesis temperature and stirring speed can increase the final purity.

A comparison of the effect of the chemical precipitation parameters between the powders obtained at lowest (N2) and highest purity (N14 and N16, with a minimum of 95% purity) is compared in Fig. 5. The purity values obtained have been verified by Rietveld refinement and shows N14 as the only powder to have attained 100 wt.% purity. The second highest level of purity obtained was for N16: with 98.89 wt.% HAp and 1.11 wt.% CaO. The lowest level of purity obtained, however, was for N2: with only 21.15 wt.% HAp evident. Instead, its predominant phase consists of 65.54 wt.% β-TCP. Comparing the chemical precipitation parameters of N2 against the more pure HAp powders (N14 and N16), therefore, demonstrates the requirement of a higher stirring speed and ripening time in obtaining increased levels of phase purity. This concept has been previously discussed in relation to studies conducted by Afshar et al. (Ref 14) confirming that the stirring speed should be high enough to prepare a good homogeneous media for preparation of HAp. Comparing N14 with N16 shows how a low calcium concentration is favoured for high levels of purity, which correlates well with that proposed by Guilietti et al. (Ref 23) who maintain that high purity levels can be attained, when precipitation is conducted at low supersaturation levels. The second factor most affecting the phase purity is a three-way interaction effect between the acid addition rate, the reaction temperature, and the atmospheric control. Seckler et al. (Ref 24) have reported that the main phase formed at room temperature is ACP with minor amounts of HAp, while the amounts of HAp present increased with an increase in temperature. The model indicates that use of a controlled inert environment and acid addition rate is favoured by use of a high reaction temperature to ensure impurities incorporated into the reaction vessel are kept at a minimum. Comparing the effect of the atmospheric control on the final purity also confirms that the presence of a controlled (inert) environment can also have a positive influence on the final phase purity.

The ripening time and reaction temperature are the third and forth most significant effects (main), respectively, and correlate well with evidence provided by Liu et al. (Ref 25) in demonstrating the significance of the ripening time with respect to purity, for the full conversion of precursor phases, such as OCP, DCPD, and ACP, to phase pure HAp, while the lifetime of the metastable amorphous precursor in aqueous solution has been reported to be a function of the reaction synthesis

temperature. With respect to purity, the only two samples in this study to satisfy regulatory requirements (min. 95%) in the order of most pure is N14 > N16.

3.2 Crystallinity Model Development

By selecting the manual regression method, the insignificant model terms ($P < 0.1$), with less than a 5% contribution were eliminated. The ANOVA results for the crystallinity showed a significant model, with R^2 (0.9141), adjusted R^2 (0.8158), and predicted R^2 (0.5510) and an adequate precision of 9.805 (supported by Fig. 2b) all obtained. The main effects for the crystallinity model were acid addition rate (V_{ac}), stirring speed (V_{st}), ripening time (t_r), controlled atmosphere (atm.), and the two-way interaction effects of acid addition rate and stirring speed ($V_{ac} * V_{st}$), acid addition rate and calcium concentration ($V_{ac} * Ca^{2+}$), reaction temperature and ripening time ($T_0 * t_r$), reaction temperature and a controlled environment (T_0 * atm.) as the most significant model terms associated with achieving high levels of crystallinity (>95%). The final mathematical models (with and without atmospheric control) are shown in Eq 10 to 12.

$$\begin{aligned}\text{Crystallinity, } X_c\ (\%) &= 72.02 + 3.14(V_{ac}) + 3.40(V_{st}) + 7.49(t_r) - 4.09(\text{atm.}) \\ &\quad - 3.44(V_{ac} * V_{st}) + 4.04\left(V_{ac} * Ca^{2+}\right) + 3.34(T_0 * t_r) \\ &\quad + 5.35(T_0 * \text{atm.}) \qquad \text{(Eq 10)}\end{aligned}$$

For an uncontrolled atmospheric environment:

$$\begin{aligned}\text{Crystallinity, } X_c\ (\%) &= +37.69018 + 4509.69603(H_3PO_4 \text{ addition rate}) \\ &\quad + 0.030509(\text{stirring speed}) + 0.11365(\text{ripening time}) \\ &\quad - 3.06155(H_3PO_4 \text{ addition rate} * \text{stirring speed}) \\ &\quad + 35.51526\left(H_3PO_4 \text{ addition rate} * Ca^{2+}\text{conc.}\right) \\ &\quad + 5.04780E - 003(\text{reaction temp} * \text{ripening time}) \qquad \text{(Eq 11)}\end{aligned}$$

For a controlled (inert) atmospheric environment:

$$\begin{aligned}\text{Crystallinity, } X_c\ (\%) &= +8.11504 + 4509.69603(H_3PO_4 \text{ addition rate}) \\ &\quad + 0.030509(\text{stirring speed}) + 0.11365(\text{ripening time}) \\ &\quad - 3.06155(H_3PO_4 \text{ addition rate} * \text{stirring speed}) \\ &\quad + 35.51526(H_3PO_4 \text{ addition rate} * Ca^{2+}\text{conc.}) \\ &\quad + 5.04780E - 003\ (\text{reaction temp} * \text{ripening time}) \qquad \text{(Eq 12)}\end{aligned}$$

The pareto chart for the crystallinity model, (Fig. 3b), highlights the order of the significant main and interaction parameter effects, which ultimately affect the crystallinity model.

The order of the level of significance of the positive effects of the chemical precipitation process parameters on crystallinity follows the order: (t_r) > (T_0 * atm.) > ($V_{ac} * Ca^{2+}$) > (V_{st}) > ($T_0 * t_r$) > (V_{ac}), while the order of the level of significance of the negative effects on the phase purity is as follows: (atm.) > ($V_{ac} * V_{st}$). Hence, to achieve high levels of crystallinity, the top four most influencing effects for control are as follows:

1.	Ripening time↑	Main effect
2.	Reaction temperature * atmospheric control↑	Two-way interaction effect
3.	Atmospheric control↓	Main effect
4.	Acid addition rate * calcium concentration↑	Two-way interaction effect

As expected, the primary factor most affecting the crystallinity confirms the ripening time as the most critical factor for controlling the resultant percentage crystallinity. The crystalline behavior as a function of ripening time is attributed to the mechanism of crystal growth in solution, since it is well known that the precipitation of particles involves nucleation and growth from a supersaturated solution. The second most important effect involves a two-way interaction effect between the reaction temperature and the atmospheric control. An increase in precipitation reaction temperature has elsewhere been reported (Ref 17, 18, 26) to further enhance the final crystallinity. Comparing the models for phase purity and

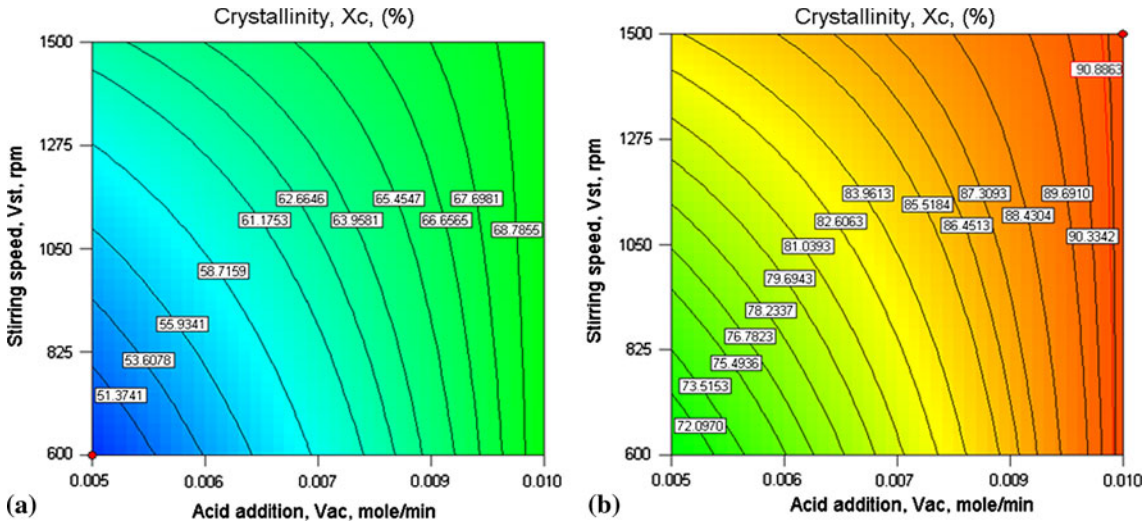

Fig. 6 2D contour plots of crystallinity at (a) a ripening time of 0.5 h and (b) a ripening time of 48 h (under a controlled environment at T_0 = 60 °C and Ca^{2+} = 2.0 M)

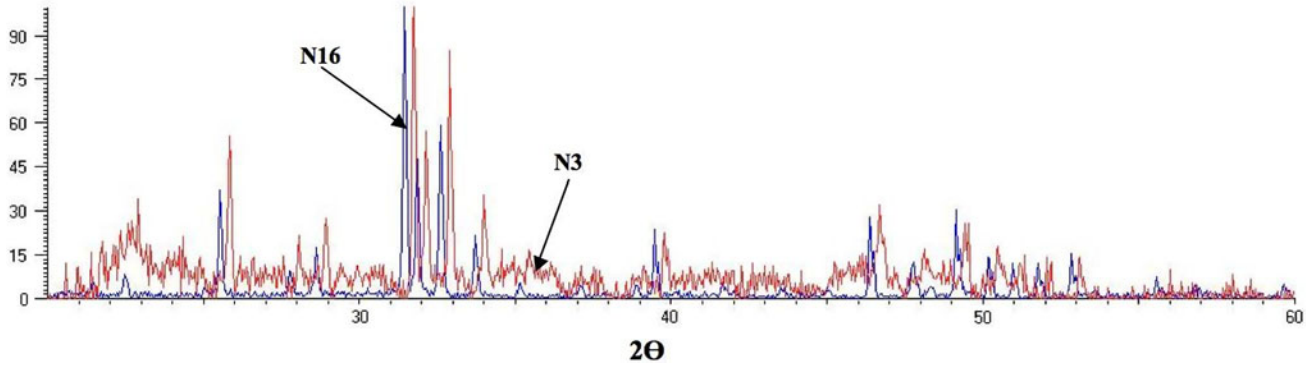

Fig. 7 2-D illustration comparing XRD spectra obtained for N3 and N16

crystallinity, it is clear that they both share the same dependency on the main effect of ripening time (t_r) and a controlled environment (atm.) to reach optimal levels for each response. The interaction effects of the acid addition rate and stirring speed ($V_{ac} * V_{st}$), acid addition rate and calcium concentration ($V_{ac} * Ca^{2+}$), reaction temperature and ripening time ($T_0 * t_r$), and reaction temperature and controlled environment ($T_0 *$ atm.) are also common interaction effects for both phase purity and crystallinity models which were found to significantly affect end result for both responses. 2-D contour plots are presented in Fig. 6(a) and (b), and highlight how the crystallinity (synthesised under a controlled inert environment) increases directly, with an increase in the acid addition rate, stirring speed and ripening time.

Figure 7 shows a 2-D illustration of the comparison in crystallinity between the XRD spectra obtained for the least and most crystalline powder samples synthesised in this study (i.e., N3 and N16). It is evident that the only powder synthesised in this study meeting the required minimum of 95% crystallinity is N16. Comparing the chemical precipitation parameters of N3 against the more crystalline HAp powders (N14 and N16) demonstrates the requirement of a higher stirring speed (V_{st}), reactant concentration (Ca^{2+} and V_{ac}), and ripening time (t_r) in obtaining increased levels of crystallinity. Comparing N14 and N16 also confirms that an increase in the reaction synthesis temperature may exert a positive influence on the final crystallinity, while the presence of a controlled environment is found to have an insignificant effect on achieving a high level of crystallinity.

3.3 Crystallite Size (L_{002} and L_{300}) Model Development

The manual regression method was used to eliminate the insignificant model terms ($P < 0.1$) with less than a 5% contribution for both crystallite size models in the 002 and 300 plane. A logit power transformation was used to develop the L_{300} model, where the response is bounded between a lower and upper limit of 10 and 140, respectively, since it possessed a ratio of maximum to minimum responses of 13.0181. A ratio greater than 10 indicates that a transformation is required. Therefore, a ratio of 2.5945 for the L_{002} model suggested that a transformation would have little effect and was not used in this case. Adequacy measures for the crystallite size models in the 002 and 300 (i.e., L_{002} and L_{300}) planes were all considered here (L_{002} of $R^2 = 0.9040$, predicted $R^2 = 0.6159$, adjusted $R^2 = 0.8199$, adequate precision = 11.085; and L_{300} of $R^2 = 0.9382$, predicted $R^2 = 0.6773$, adjusted $R^2 = 0.8676$, adequate precision = 19.161) and supported by Fig. 2(c) and (d).

The main effects for the crystallite size model for the L_{002} plane were the stirring speed (V_{st}), ripening time (t_r), calcium concentration (Ca^{2+}), atmospheric control (atm.), and the two-way interaction effects of acid addition rate and ripening time ($V_{ac} * t_r$), reaction temperature and ripening time ($T_0 * t_r$), and reaction temperature and atmospheric control ($T_0 *$ atm.). On the other hand, the significant main effects on the crystallite size in the 300 plane were the acid ripening time (t_r), acid addition rate (V_{ac}), and stirring speed (V_{st}), while two-way interactions between the acid addition rate and the reaction temperature ($V_{ac} * T_0$), acid addition rate and calcium concentration ($V_{ac} * Ca^{2+}$), acid addition rate and atmospheric environment ($V_{ac} *$ atm.), and reaction temperature and ripening time ($T_0 * t_r$) is also found to be an influencing factor for this response. A three-way interaction effect between the acid addition rate, reaction temperature, and the atmospheric environment ($V_{ac} * T_0 *$ atm.) was also noted. The final mathematical models for the crystallite size response, L_{002}, are shown in Eq 13 to 15, and for L_{300} presented in Eq 16 to 18.

$$\begin{aligned}\text{Crystallite size, } L_{002}\ (\text{nm}) &= 64.96 + 6.54(V_{st}) - 3.94(t_r) + 7.02\left(Ca^{2+}\right) \\ &\quad + 9.23(\text{atm.}) + 6.77(V_{ac} * t_r) \\ &\quad + 7.32(T_0 * t_r) + 4.11(T_0 * \text{atm.})\end{aligned} \quad \text{(Eq 13)}$$

For an uncontrolled atmospheric environment:

$$\begin{aligned}\text{Crystallite size, } L_{002}\ (\text{nm}) &= +44.94738 + 0.014535(\text{stirring speed}) \\ &\quad - 0.87066(\text{ripening time}) + 7.39386\left(Ca^{2+}\ \text{conc.}\right) \\ &\quad + 40.94013(H_3PO_4\ \text{addition rate} * \text{ripening time}) \\ &\quad + 9.94218\text{E} - 003(\text{reaction temp} * \text{ripening time})\end{aligned} \quad \text{(Eq 14)}$$

For a controlled (inert) atmospheric environment:

$$\begin{aligned}\text{Crystallite size, } L_{002}\ (\text{nm}) &= +46.96590 + 0.014535(\text{stirring speed}) \\ &\quad - 0.87066(\text{ripening time}) + 7.39386\left(Ca^{2+}\ \text{conc.}\right) \\ &\quad + 40.94013(H_3PO_4\ \text{addition rate} * \text{ripening time}) \\ &\quad + 9.94218\text{E} - 003(\text{reaction temp} * \text{ripening time})\end{aligned} \quad \text{(Eq 15)}$$

$$\begin{aligned}&\text{Logit (crystallite size, } L_{300}\text{ (nm))}\\&= \text{Ln}[(\text{crystallite size}, L_{300} - 10.00)/\\&\quad (140.00\ \text{Crystallite size, } L_{300})] = +0.15 - 0.77(V_{ac})\\&\quad + 0.65(V_{st}) - 0.85(t_r) + 0.52(V_{ac} * T_0)\\&\quad - 0.89\left(V_{ac} * Ca^{2+}\right) - 0.71(V_{ac} * \text{atm.})\\&\quad + 0.59(T_0 * t_r) + 0.62(V_{ac} * T_0 * \text{atm.})\end{aligned} \quad \text{(Eq 16)}$$

For an uncontrolled atmospheric environment:

$$\begin{aligned}&\text{Logit (crystallite size, } L_{300}\text{(nm))}\\&= \text{Ln}[(\text{crystallite size, } L_{300} - 10.00)/\\&\quad (140.00 - \text{crystallite size, } L_{300})]\\&= +1.81027 - 235.26182(H_3PO_4\text{ addition rate}\\&\quad + 1.45519\text{E} - 003 * \text{stirring speed})\\&\quad - 0.071007(\text{ripening time})\\&\quad - 1.73988(H_3PO_4\text{ addition rate} * \text{reaction temp})\\&\quad - 12.33184\left(H_3PO_4\text{ addition rate} * Ca^{2+}\text{ conc.}\right)\\&\quad + 8.76279\text{E} - 004(\text{reaction temp} * \text{ripening time})\end{aligned} \quad \text{(Eq 17)}$$

For a controlled (inert) atmospheric environment:

$$\begin{aligned}&\text{Logit (crystallite size, } L_{300}\text{(nm))}\\&= \text{Ln}[(\text{crystallite size, } L_{300} - 10.00)/\\&\quad (140.00 - \text{crystallite size, } L_{300})]\\&= +1.81027 - 349.78734(H_3PO_4\text{ addition rate})\\&\quad + 1.45519\text{E} - 003(\text{stirring speed})\\&\quad - 0.071007(\text{ripening time})\\&\quad - 1.54575(H_3PO_4\text{ addition rate} * \text{reaction temp})\\&\quad - 12.33184\left(H_3PO_4\text{ addition rate} * Ca^{2+}\text{ conc.}\right)\\&\quad + 8.76279\text{E} - 004(\text{reaction temp.} * \text{ripening time})\end{aligned} \quad \text{(Eq 18)}$$

The pareto charts for the crystallite size models for both the L_{002} and L_{300} planes, as illustrated in Fig. 3(c) and (d), highlight the most significant parameters with either a positive or negative effect on each model. The order of the level of significance of the positive effects on the L_{002} model, from the most significant, follows the order: (atm.) > (T_0 * t_r) > (Ca^{2+}) > (V_{ac} * t_r) > (V_{st}) > (T_0 * atm.), while the only negative effect to significantly affect the L_{002} model is the ripening time (t_r). The order of the level of significance of the most significant positive effects on the L_{300} model follows the order: (V_{st}) > (V_{ac} * T_0 * atm.) > (T_0 * t_r) > (V_{ac} * T_0), while the order of the level of most significant negative effects follows the order: (V_{ac} * atm.) > (t_r) > (V_{ac}) > (V_{ac}* atm.) for the L_{002} model.

Hence, to achieve high levels of crystallite size in both planes, the top four most influencing effects for controlling both responses are as follows:

For crystallite size, L_{002}	
1. Atmospheric environment↑	Main effect
2. Reaction temperature * ripening time↑	Two-way interaction effect
3. Calcium concentration↑	Main effect
4. Acid addition rate * ripening time↑	Two-way interaction effect

For crystallite size, L_{300}	
1. Acid addition rate * calcium concentration↓	Two-way interaction effect
2. Ripening time↓	Main effect
3. Acid addition rate↓	Main effect
4. Acid addition rate * atmospheric environment↓	Two-way interaction effect

First, the top four most influencing effects are not similar in both the cases of crystallite size for the two plane investigated. The factor most affecting the crystallite size in the 002 plane is the use of a controlled inert environment. The model dictates that the implementation of this parameter will increase the crystallite size in this plane. This theory is in good agreement with a similar finding by Smiciklas et al. (Ref 17) where a resulting increase of crystallite size for this plane was also reported, from the use of an inert atmosphere. The second most influencing factor for this plane is the two-way interaction effect between the reaction temperature and the ripening time. Smiciklas et al. (Ref 17) examined the effect of both factors as a main effect and reported that an increase in both contributed to an increase in the crystallite size for this plane. The third most influencing factor is the calcium concentration, for which an increase of this parameter can also produce a larger crystallite size for this plane. However, in comparison an increase of calcium concentration (interacting with the acid addition rate) can reduce the crystallite size in the 300 plane. Both results agree well with findings reported in a similar study (Ref 17). The fourth most influencing factor is the two-way interaction between the acid addition rate and the ripening time. Again, it has reported that both of these factors investigated as main effects can increase the crystallite size for this plane. In contrast, a reduction of all four most influencing factors can acquire a larger crystallite size for the 300 plane. These findings correlate well with those reported by Smiciklas et al. (Ref 17), with the exception of ripening time, where it was reported that an increase was required for an increase in crystallite size for the 300 plane.

3.4 Lattice Parameter Ratio Model Development

Selecting the backward regression method allowed for the elimination of the insignificant model terms, automatically. The ANOVA results revealed: R^2 (0.9578), adjusted R^2 (0.9209), and predicted R^2 (0.8312), for the reduced linear model relating to the response of the lattice parameter ratio (a/c). For this model, the "Prob. > F" value does not exceed 0.1, which indicates that the models are statistically significant. Since the adequate precision compares the range of the predicted value at the design points to the average prediction error, the value of an adequate precision of 16.042 indicates adequate model discrimination. Figure 2(e) shows the relationship between the actual and the predicted values of the lattice parameter ratio. This figure indicates that the developed model is adequate, since the residuals in the prediction of each response are small, with the residuals tending to be close to the diagonal line. The range of values appears to lie in three clusters between a minimum of ~1.369, an average of ~1.374 and a maximum value of ~1.378.

The ANOVA for the lattice parameter ratio (a/c) model shows that all the chemical precipitation parameters, with the exclusion of atmospheric control have a significant effect on the resulting a/c ratio model, either as a main or interaction effect

with another parameter. The main effects of the reaction temperature (T_0), stirring speed (V_{st}), ripening time (t_r), calcium concentration (Ca^{2+}), and the two-way interaction effects of acid addition rate and reaction temperature ($V_{ac} * T_0$), acid addition rate and stirring speed ($V_{ac} * V_{st}$), acid addition rate and calcium concentration ($V_{ac} * Ca^{2+}$) are the most significant model terms associated with altering the lattice parameter ratio. It is clear that all the significant interaction effects included in the model involve the acid addition rate as an influencing variable to affect the resulting a/c ratio and hence it's crystallographic structure. The final mathematical models for the lattice parameter ratio response are shown in Eq 19 and 20.

Coded factor: a/c ratio

$$= 1.37 - 7.563E-004(T_0) - 1.731E-003(V_{st}) - 2.306E-003(t_r) + 5.812E-004\left(Ca^{2+}\right) + 5.063E-004(V_{ac} * T_0) - 4.937E-004(V_{ac} * V_{st}) - 6.812E-004\left(V_{ac} * Ca^{2+}\right) \quad \text{(Eq 19)}$$

Actual factor: a/c ratio

$$= +1.38138 - 1.26577E-004(\text{Reaction temp}) - 1.22065E-006(\text{stirring speed}) - 9.71053E-005(\text{ripening time}) + 2.61393E-003\left(Ca^{2+}\ \text{conc.}\right) + 0.011835(H_3PO_4\ \text{addition rate} * \text{reaction temp}) - 3.50210E-004(H_3PO_4\ \text{addition rate} * \text{stirring speed}) - 0.26694\left(H_3PO_4\ \text{addition rate} * Ca^{2+}\ \text{conc.}\right) \quad \text{(Eq 20)}$$

The pareto chart for the lattice parameter ratio model, as illustrated in Fig. 3(e), highlights the most significant parameters affecting the model. The order of the level of significance of the positive effects of the chemical precipitation process parameters on the a/c ratio follows the order: $(Ca^{2+}) > (V_{ac} * T_0)$, while the order of the level of significance of the negative effects on the lattice parameter ratio is as follows: $(t_r) > (V_{st}) > (T_0) > (V_{ac} * Ca^{2+}) > (V_{ac} * V_{st})$. Although, if a low lattice parameter ratio is required, the top four most influencing effects for controlling this response are as follows:

1.	Ripening time↑	Main effect
2.	Stirring speed↑	Main effect
3.	Reaction temperature↑	Main effect
4.	Acid addition rate * calcium concentration↑	Two-way interaction effect

The factor most affecting the lattice parameter ratio is the ripening time. Increasing the ripening time indicates that a decrease in the ratio can be achieved, representing a contraction in the *a* direction and an expansion in the *c* direction. On the other hand, β-TCP is promoted with an expansion in the *a* direction and a contraction in the *c* direction (Ref 24). 2-D contour plots are presented in Fig. 8(a) and (b), and highlight the negative influence of decreasing both the reaction synthesis temperature and the acid addition rate.

3.5 Particle Size Model Development

Selecting the backward regression method allowed for the elimination of the insignificant model terms, automatically. The ANOVA results revealed: R^2 (0.9790), adjusted R^2 (0.9550), and predicted R^2 (0.8903), relating to the particle size response. For this model, the "Prob. > F" value does not exceed 0.05, which indicates that the model developed is statistically significant. In this case, the value of adequate precision is 18.284 and represents adequate model discrimination (Fig. 2f). The ANOVA indicates that for the particle size model, all the chemical precipitation parameters have a significant effect on the resulting model, either as a main or interaction effect with another parameter. The main effects of the reaction temperature (T_0), stirring speed (V_{st}), calcium concentration (Ca^{2+}), atmospheric control (atm.), and the two-way interaction effects of acid addition rate and reaction temperature ($V_{ac} * T_0$), acid addition rate and calcium concentration ($V_{ac} * Ca^{2+}$), acid addition rate and atmospheric environment ($V_{ac} *$ atm.) and the reaction temperature and ripening time ($T_0 * t_r$) are the most

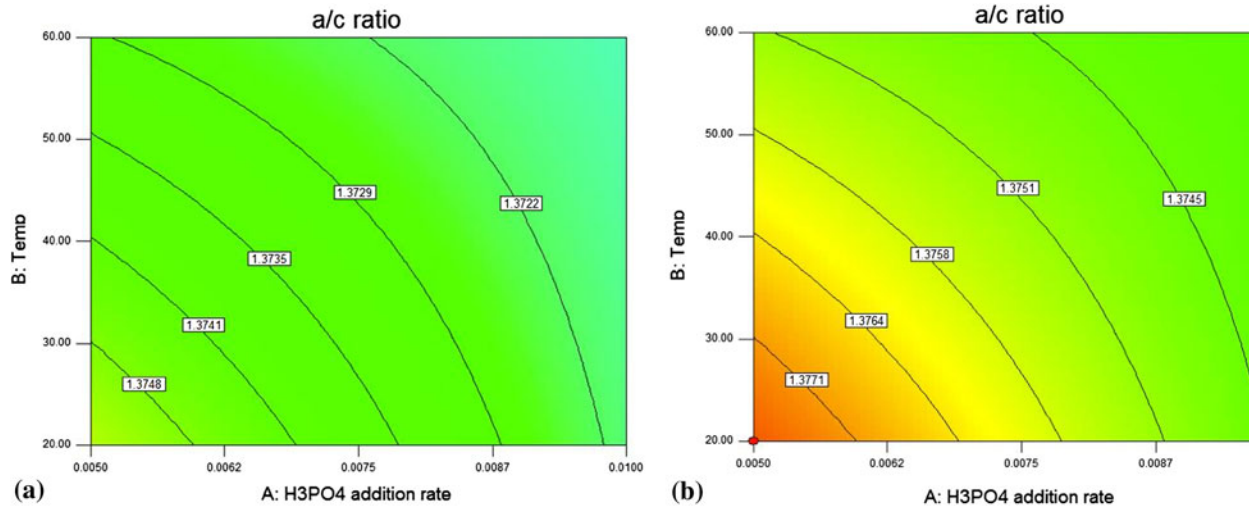

Fig. 8 Effect of V_{ac} and T_0 on the lattice parameter ration at (a) a ripening time of 48 h and (b) a ripening time of 0.5 h, (under a controlled environment at V_{st} = 1500 rpm and Ca^{2+} = 2.0 M

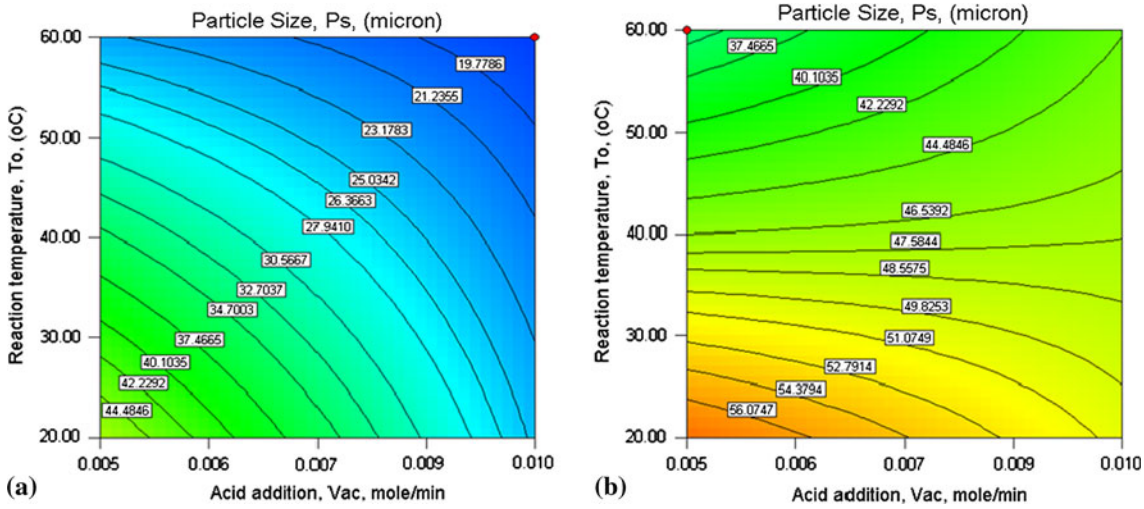

Fig. 9 2D contour plots of particle size at (a) a Ca^{2+} conc. of 2.0 M and (b) a Ca^{2+} conc. of 0.1 M (under a controlled environment at V_{st} = 1500 rpm and t_r = 48 h)

significant model terms associated with affecting the particle size. The final mathematical model for the particle size response in terms of coded factors (Eq 21), and actual factors (Eq 22 and 23) for the response on the particle size, under an uncontrolled and inert atmospheric environment, are given as:

$$\begin{aligned}&\text{Particle size}, P_s\ (\mu\text{m})\\&= 39.34 - 9.64(T_0) - 2.51(V_{st}) - 9.32\left(Ca^{2+}\right) + 2.03(\text{atm.})\\&\quad + 4.32(V_{ac} * T_0) - 3.67\left(V_{ac} * Ca^{2+}\right) - 3.54(V_{ac} * \text{atm.})\\&\quad + 2.19(T_0 * t_r)\end{aligned} \quad \text{(Eq 21)}$$

For an uncontrolled atmospheric environment:

$$\begin{aligned}&\text{Particle size}, P_s\ (\mu\text{m})\\&= +62.12231 - 0.92449(\text{reaction temp}) - 5.56806\text{E}\\&\quad - 003(\text{stirring speed}) + 4.14248\left(Ca^{2+}\ \text{conc.}\right)\\&\quad + 59.20540(H_3PO_4\ \text{addition rate} * \text{reaction temp})\\&\quad - 1860.13802\left(H_3PO_4\ \text{addition rate} * Ca^{2+}\ \text{conc.}\right)\\&\quad + 5.50000\text{E} - 005(\text{reaction temp} * \text{ripening time})\end{aligned} \quad \text{(Eq 22)}$$

For a controlled (inert) atmospheric environment:

$$\begin{aligned}&\text{Particle size}, P_s\ (\mu\text{m})\\&= +87.39981 - 0.92449(\text{reaction temp}) - 5.56806\text{E}\\&\quad - 003(\text{stirring speed}) + 4.14248\left(Ca^{2+}\ \text{conc.}\right)\\&\quad + 59.20540(H_3PO_4\ \text{addition rate} * \text{reaction temp})\\&\quad - 1860.13802\left(H_3PO_4\ \text{addition rate} * Ca^{2+}\ \text{conc.}\right)\\&\quad + 5.50000\text{E} - 005(\text{reaction temp} * \text{ripening time})\end{aligned} \quad \text{(Eq 23)}$$

The pareto chart for the particle size model, as illustrated in Fig. 3(f), highlights the most significant parameters affecting the model. The order of the level of significance of the positive effects of the chemical precipitation process parameters on the actual particle size follows the order: $(V_{ac} * T_0) > (T_0 * t_r) >$ (atm.) while the order of the level of significance of the negative effects on the lattice parameter ratio is as follows: $(T_0) > (Ca^{2+}) > (V_{ac} * Ca^{2+}) > (V_{ac} * \text{atm.}) > (V_{st})$. Hence, if low particle sizes are to be obtained, the top four most influencing effects for controlling this response are as follows:

1.	Reaction temperature↑	Main effect
2.	Calcium concentration↑	Main effect
3.	Acid addition rate * reaction temperature↓	Two-way interaction effect
4.	Acid addition rate * calcium concentration↑	Two-way interaction effect

The top two most influencing factors affecting the particle size is the reaction temperature and calcium concentration, indicating an increase in both factors can result in a decrease for this response. However, the third most influencing effect suggests that the reaction temperature is also involved in an interaction effect with the acid addition rate and a reduction in both can yield higher powder particle sizes, as expected from literature (Ref 27). The fourth most significant effect involves another two-way interaction between the acid addition rate and the calcium concentration, requiring an increase for a reduction in particle size. Contour plots examining the most significant effects are shown in Fig. 9. These plots indicate that a larger particle size results when the addition rate of the acid is lowered and this phenomenon agrees well with that hypothesized by Afshar et al. (Ref 14). The model also demonstrates that the lower acid addition rate coupled with a lower synthesis temperature is favoured in producing larger size HAp particles. However, the calcium concentration is shown to also play a major role in determining the final particle size.

In summary, all the factors studied have an impact (of minor and major significance) on one or more of the responses investigated, either as a main or interaction effect. Both the ripening time and stirring speed significantly affect the majority of the responses (effecting five responses), with the reaction temperature also having a significant effect on the purity, a/c ratio and particle size. However, the interaction effect of the acid addition rate and calcium concentration is also shown to effect three of the responses, but the inclusion of these factors

Table 5 Summary of findings after the screening stage of experimental design

Effects	Responses					
	↑Purity, X_p	↑Crystallinity, X_c	↑Crystallite size		↓a/c ratio	↓Particle size, P_s
			L_{002}	L_{300}		
Main						
(A) V_{ac}				↓		
(B) T_0	↑				↑	↑
(C) V_{st}				↑	↑	
(D) t_r	↑	↑		↓	↑	
(E) Ca^{2+}			↑			↑
(F) atm.		↓	↑			
Interaction						
A * C	↑					
A * B						
A * C						
A * D			↑			
A * E		↑			↑	↑
A * F						
B * D			↑			
B * F		↑				
A * B * F	↑					

(to attain this interaction) would produce an optimization design (Box-Behnken) taking account of all the factors (with the exclusion of atmospheric control), analogous to the screening design (Fractional-Factorial) and this would require a minimum of 45 experiments instead of the 17 experiments used (using 5 center points in both instances).

4. Conclusion

The Fractional-Factorial (Res IV) experimental design was applied to screen a large number of variables in synthesis of HAp by the chemical precipitation method, and to analyze their influence on HAp physicochemical properties. The critical responses for design control in this study are primarily the HAp phase purity and crystallinity (both > 95% to aid in satisfying regulatory requirements) and particle size (<100 μm) for plasma spraying application) obtained as a result of varying the factors between the two levels investigated. A reduced lattice parameter ratio would indicate a decrease in the *a* direction and an increase in the *c* direction, which appears more favorable than an increased level of a/c ratio, which is shown to effectively decrease the crystallinity response (Ref 28). Table 5 outlines the effect (main and interaction) of the top four most significant factors influencing the final desired responses, based on the models developed in the preceding sections. Hence, the increase or decrease of the top four most influencing main and interaction effects to obtain increased levels of phase purity, crystallinity and crystallite size, while a decrease the a/c ratio and ↓particle size are depicted in Table 5. T_0 achieve these desired responses, it appears that an increase in the majority of the main factors is required. Use of a controlled atmospheric environment is compromised between requirement for increased phase purity and crystallinity. However, experiment N16 demonstrates that its synthesis with a controlled environment results in values >95% for both responses. Calcium concentration and acid addition rate, however appear to have little effect on the final powder characteristics, with the acid addition rate controlling only the crystallographic properties in comparison to the remaining three factors (that is, reaction temperature, stirring speed and ripening time).

Acknowledgment

This study is supported under the EMBARK Initiative Scheme by the Irish Research Council for Science and Engineering (IRCSET).

References

1. V. Palka, E. Postrkova, and H.K. Koerten, Some Characteristics of Hydroxylapatite Powder Particles after Plasma Spraying, *Biomaterials*, 1998, **19**(19), p 1763–1772
2. S.J. Kalita, S. Bose, H.L. Hosick, and A. Bandyopadhyay, $CaO–P_2O_5–Na_2O$-Based Sintering Additives for Hydroxyapatite (HAp) Ceramics, *Biomaterials*, 2003, **25**(12), p 2331–2339
3. S.W.K. Kweh, K.A. Khor, and P. Cheang, The Production and Characterization of Hydroxyapatite (HA) Powders, *J. Mater. Process. Technol.*, 1999, **89–90**, p 373–377
4. A.D. Papargyris, A.I. Botis, and S. Papargyri, Synthetic Routes for Hydroxyapatite Powder Production, *Key Eng. Mater.*, 2002, **206–213**, p 83–86
5. S. Koutsoploulos, Synthesis and Characterization of Hydroxyapatite Crystals: A Review Study on the Analytical Methods, *J. Biomed. Mater. Res.*, 2002, **15**, p 600–612
6. N. Kivrak and C. Tas, Synthesis of Calcium Hydroxyapatite Tricalcium Phosphate (HA-TCP) Composite Bioceramic Powders and Their Sintering Behavior, *J. Am. Ceram. Soc.*, 1998, **81**, p 2245–2252
7. J.L. Xu, K.A. Khor, Z.L. Dong, Y.W. Gu, R. Kumar, and P. Cheang, Preparation and Characterization of Nano-Sized Hydroxyapatite Powders Produced in a Radio Frequency (rf) Thermal Plasma, *Mater. Sci. Eng. A*, 2004, **374**, p 101–108
8. R. Kumar, P. Cheang, and K.A. Khor, RF Plasma Processing of Ultra-Fine Hydroxyaptite Powders, *Mater. Process. Technol.*, 2001, **113**, p 456–462
9. U.S. Food and Drug Administration, *Calcium Phosphate (Ca-P) Coating Draft Guidance for Preparation of FDA Submissions for Orthopaedic and Dental Endosseous Implants*, 1992
10. ASTM F1609, *Standard Specification for Calcium Phosphate Coatings for Implantable Materials*, American Society for Testing and Materials, 2003
11. ISO 13779-1, *Implants for Surgery: Hydroxyapatite—Part 1: Ceramic Hydroxyapatite*, International Standards Organisation, 2000
12. ASTM F1185, *Standard Specification for Composition of Hydroxylapatite for Surgical Implants*, American Society for Testing and Materials, 2003
13. T.S.S. Kumar, I. Manjubala, and J. Gunasekaran, Synthesis of Carbonated Calcium Phosphate Ceramics Using Microwave Irradiation, *Biomaterials*, 2000, **21**, p 1623–1629
14. A. Afshar, M. Ghorbani, N. Ehsani, M.R. Saeri, and C.C. Sorrell, Some Important Factors in the Wet Precipitation Process of Hydroxyapatite, *Mater. Lett.*, 2003, **57**, p 197–202
15. M.R. Saeri, A. Afshar, M. Ghorbani, N. Ehsani, and C.C. Sorrell, The Wet Precipitation Process of Hydroxyapatite, *Mater. Lett.*, 2003, **57**, p 4064–4069
16. J.F. Conn and L.A. Jessen Process for Producing Hydroxyapatite, Patent Number: US 4,324,772, 1982
17. I. Smiciklas, A. Onjia, and S. Raicevic, Experimental Design Approach in the Synthesis of Hydroxyapatite by Neutralization Method, *Sep. Purif. Technol.*, 2005, **44**, p 97–102
18. S. Lazic, S. Zec, N. Miljevic, and S. Milonjic, The effect of Temperature on the Properties of Hydroxyapatite Precipitated from

Calcium Hydroxide and Phosphoric Acid, *Thermochim. Acta*, 2001, **374**, p 13–22
19. R. Kumar, K.H. Prakash, P. Cheang, and K.A. Khor, Temperature Driven Morphological Changes of Chemically Precipitated Hydroxyapatite Nanoparticles, *Langmuir*, 2004, **20**, p 5196–5200
20. A. Tampieri, G. Celotti, S. Sprio, and C. Mingazzini, Characteristics of Synthetic Hydroxyapatites and Attempts to Improve Their Thermal Stability, *Mater. Chem. Phys.*, 2000, **64**, p 54–61
21. K. Rogers, *The Use of Diffraction for the Analysis of Biomaterials*, 2nd Annual Biomaterials Workshop, Cranfield University, UK, 2004
22. Design-Expert Software, Version 7.1, User's guide, Technical Manual, Stat-Ease Inc., Minneapolis, MN, 2007
23. M. Giulietti, M.M. Seckler, S. Derenzo, M.I. Re, and E. Cekinski, Industrial Crystallisation and Precipitation from Solutions: State of the Technique, *Brazil. J. Chem. Eng.*, 2001, **15**, p 423–440
24. M.M. Seckler, M. Danese, S. Derenzo, J.V. Valarelli, M. Giulietti, and R. Rodríguez-Clemente, Influence of Process Conditions on Hydroxyapatite Crystallinity Obtained by Direct Crystallization, *Mater. Res.*, 1999, **2**(2), p 59–62
25. C. Liu, Y. Huang, W. Shen, and J. Cui, Kinetics of Hydroxyapatite Precipitation at pH 10 to 11, *Biomaterials*, 2001, **22**, p 301–306
26. Y.X. Pang and X. Bao, Influence of Temperature, Ripening Time and Calcination on the Morphology and Crystallinity of Hydroxyapatite Nanoparticles, *J. Eur. Ceram. Soc.*, 2003, **23**, p 1697–1704
27. J. Liu, X. Ye, H. Wang, M. Zhu, B. Wang, and H. Yan, The Influence of pH and Temperature on the Morphology of Hydroxyapatite Synthesised by Hydrothermal Method, *Ceram. Int.*, 2003, **29**, p 629–633
28. L.L. Hench, J. Wilson, An Introduction to Bioceramics, *Advanced Series in Ceramics*, Vol 1 World Scientific Publishing Co. Pte. Ltd., London, Hong Kong, Singapore, 1998, p 139–80